ELSEVIER

Journal of Power Sources 103 (2002) 253–264

JOURNAL OF POWER SOURCES

www.elsevier.com/locate/jpowsour

In situ analysis of the interfacial reactions between MCMB electrode and organic electrolyte solutions

Ken-ichi Morigaki*

Matsushita Electric Industrial Co. Ltd., Battery Research and Development Center, 1 Matsushita-cho, C/o Room, Moriguchi, Osaka 570-8511, Japan

Received 31 July 2000; received in revised form 20 April 2001; accepted 9 July 2001

Abstract

The interfacial phenomena between graphite (mesocarbon-microbeads (MCMB)) electrode and organic electrolyte solution were analyzed by in situ atomic force microscopy (AFM) and Fourier transform infrared (FTIR) spectroscopy. The influence of lithium salts (anion species), $LiPF_6$, $LiBF_4$, and $LiClO_4$, on the interfacial reaction, including lithium intercalation into graphite, was investigated in EC + DMC solutions. In situ AFM observation disclosed that morphological changes are quite different from one another depending on the kind of lithium salt (anion). A large expansion of MCMB particle was observed particularly in $LiPF_6$/EC + DMC. An expansion of MCMB particle started above 1.0 V versus Li/Li^+ and this expansion seemed to be caused by the decomposition of ternary graphite intercalation compound (GIC) ($C_nLi(sol)_y$), because the expansion remained after de-intercalation of lithium. IRAS spectra of each electrolyte solution showed different behaviors and different reduction products of solvents. double modulation FTIR (DMFTIR) spectra on graphite electrode, which emphasize the surface species, indicated relatively small changes after cathodic polarization. Therefore, the observed morphological changes were caused mainly by the expansion of graphene layers and not by the precipitation of reduction products.

Keywords: Lithium-ion battery; Intercalation; Interfacial reaction; In situ analysis; FTIR; AFM

1. Introduction

The development of rechargeable lithium-ion batteries has been remarkably proceeding in recent years. Lithium-ion batteries use graphite or amorphous carbon for the negative electrodes to apply intercalation reaction or insertion reaction of lithium ions. Many researchers are studying new carbonaceous materials to improve battery performance, such as a higher specific energy or a longer cycle life. One of the important factors for improvement is the interfacial reaction between the negative electrode (graphite or amorphous carbon) and organic electrolyte solution in a battery system. The interfacial reaction includes the surface reaction making surface passive layers, the irreversible capacity loss at the first cycle, and the effect of solvent species on lithium intercalation into graphite. In spite of impressive development of lithium-ion batteries, the interfacial reaction remains as an obscure and unrevealed problem. It is generally accepted that solvents decompose to form surface passive layers, which are lithium ion conductive films, on a carbon electrode during the first charging process in lithium-ion batteries [1–3]. Although it seems that the reduction products of solvents and the surface passive layer on graphite electrode are similar to those of lithium electrode, the lithium intercalation into graphite cannot occur enough in a few electrolyte solutions, such as γ-butyrolactone, propylene carbonate (PC) and ethers which are stable and useful solvents for lithium metal electrodes. It was reported that the decomposition of PC on graphite electrode occurs at higher potentials (about 0.8 V versus Li/Li^+) leading exfoliation and destruction of graphene layer [4–6]. Only a few groups pay attention to the interfacial reaction or the film formation on graphite electrode. Aurbach and co-workers compared the surface chemistry of lithium and graphite electrodes in many electrolyte solutions [7–9]. They reported that lithium salts used in lithium battery systems are divided into two groups: non-reactive salts, such as $LiClO_4$ and $LiAsF_6$, and reactive salts, such as $LiBF_4$, $LiPF_6$ and $LiSO_3CF_3$. When the non-reactive salts were used, the interface formed between lithium and electrolyte solution was stable, while in the case of the reactive salts the interfacial resistance was high and increased upon storage [9]. Other studies using ex situ X-ray photoelectron

* Fax: +81-6-6998-3179.
E-mail address: pan22005@pas.mei.co.jp (K.-i. Morigaki).

0378-7753/02/$ – see front matter
PII: S0378-7753(01)00858-8

spectroscopy (XPS) reported that the surface layer on lithium after immersion in electrolyte solution containing $LiPF_6$ or $LiBF_4$ was covered with LiF and Li_2O. On the other hand, the surface layer consisted of Li_2CO_3, Li_2O, LiOH, lithium alkylcarbonate and small amount of LiCl in the $LiClO_4$-solution [10,11].

The analysis on graphite surface in lithium-ion batteries involves the same difficulties as those in lithium metal batteries; that is, the amount of interfacial reaction products is very small and the products are very sensitive to H_2O, CO_2, and O_2 in the air. This instability of products demands in situ analysis in studies about the surface and interfacial reaction of lithium-ion batteries. Fourier transform infrared (FTIR) spectroscopy is one of the useful methods for in situ analysis of interfacial reactions. The surface reactions on graphite electrode in many organic electrolyte solutions have been investigated by in situ and ex situ FTIR spectroscopy [12–15]. Another useful method for in situ analysis is atomic force microscopy (AFM) [16]. AFM is capable of observing the surface morphology under high vacuum, air atmosphere, and in liquid including electrolyte solutions. The author has shown that AFM observation is a useful method for in situ analysis of lithium surface and reported a mosaic-like nano-structure of lithium surface [17,18]. Morphological studies on graphite electrode have been investigated in organic electrolyte solutions by electrochemical AFM or STM [19–22].

In this study, surface reaction on graphite electrode during intercalation/de-intercalation is investigated by in situ AFM and FTIR. The graphite composite electrodes consist of mesocarbon-microbeads (MCMB) and stylene-butadiene rubber (SBR) binder resin. The electrolyte solutions are ethylene carbonate (EC) + dimetyl carbonate (DMC) mixed solutions containing 1 mol dm^{-3} $LiPF_6$, $LiBF_4$ or $LiClO_4$. The effects of lithium salts (anion species) on the interfacial reactions are compared. Two methods of in situ FTIR spectroscopy, infrared reflection absorption spectroscopy (IRAS) and double modulation FTIR (DMFTIR) spectroscopy [23,24], are used in the present study.

2. Experimental

EC and DMC of battery grade (Mitsubishi Chemical), and $LiPF_6$ and $LiBF_4$ of battery grade (Stella Chemifa), and $LiClO_4$ of battery grade (Tomiyama Chemical) were used as received. The electrolyte solutions used in this study were EC + DMC (1:1 by volume) containing 1 mol dm^{-3} $LiPF_6$, $LiBF_4$, and $LiClO_4$. The water content of each solution was less than 50 ppm. Composite graphite electrodes were prepared by coating graphite paste on one face of copper rod (∅ 8 mm), dried at 110°C in vacuum and polished with soft cloths. The graphite paste consisted of MCMB (from Osaka gas, mean grain size; 4 μm), SBR as a binder, carboxyl methyl-cellulose and water. Lithium served as the counter and reference electrodes in test cells.

IRAS and DMFTIR spectroscopy were carried out using a Mattson RS-2 spectrometer. The FTIR system and a test cell are described in Figs. 1 and 2, respectively. IRAS was performed using p-polarized IR beam to investigate the reaction of electrolyte solutions on the graphite electrodes. DMFTIR spectroscopy was performed using p-polarized and s-polarized IR beams modulated by a photoelastic modulator (PEM-90, Hinds) to investigate the interfacial reaction at the graphite electrode. The DMFTIR spectra were collected with a real-time sampling electronics (Mattson). A detector signal consists of an ac component corresponding to $(I_p - I_s)$ and a dc component corresponding to $(I_p + I_s)$, where I_p and I_s are detected intensities of the p- and s-polarized beam. As described in a previous paper [25], $(I_p - I_s)/(I_p + I_s)$ is given as a DMFTIR spectrum. The main advantage of this technique is that $(I_p - I_s)$, which contains the absorption spectra on the electrode surface, is amplified directly with a real-time sampling electronics before digitization, resulting in a high signal-to-noise ratio. The center frequency of DMFTIR spectroscopy was set at 1200 cm^{-1} and the resolution of spectra was 2 cm^{-1}. A total of 100 FTIR measurement scans were accumulated. In situ AFM and lateral force microscopy (LFM) measurements were performed by means of a TMX-1000 system (Topometrix).

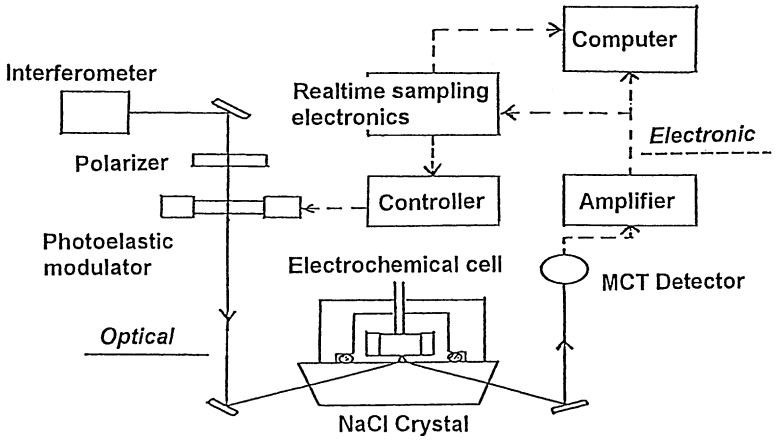

Fig. 1. Schematic diagram of the optical and electronic configuration for in situ FTIR measurements.

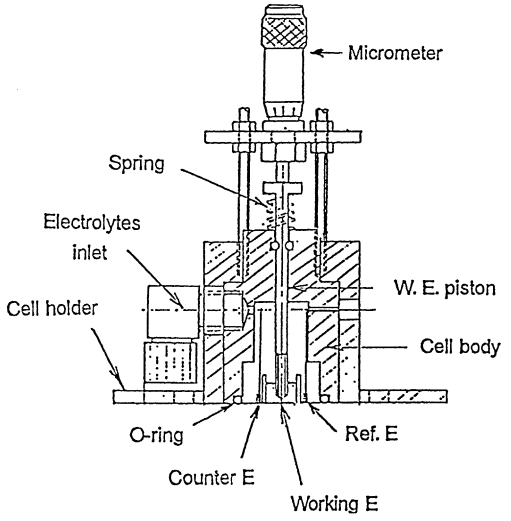

Fig. 2. Spectroelectrochemical cell for the external reflectance mode of in situ FTIR spectroscopy.

LFM image reflects the bending and twisting of the cantilever when the cantilever moves on the surface of sample, and indicates the different friction force corresponding to the various surface species with surface topography. Therefore, LFM measurements are useful to investigate the degree of surface homogeneity and uniformity. The AFM system is the same as described in the previous papers [17,18].

The working electrode was polarized with a potentio/galvanostat system HA-301/HB-104 (Hokuto denko). First, the potential of graphite electrode was polarized to 2.0 V versus Li/Li^+ from open circuit voltage (OCV; around 3 V), kept at 2.0 V until the current decreased below 20 μA, and then in situ measurement (AFM or FTIR) was performed. After measurement, the potential of working electrode was polarized to 0 V with a step width of 0.5 V, and then the potential was returned to 1.0 V with the same step width. Polarization cycle (1.0 ↔ 0 V) was repeated three times. In AFM experiments, the lowest potential of graphite electrode was set at 0.05 V versus Li/Li^+ to avoid lithium deposition. All experiments were performed in a dry-air atmosphere at room temperature.

3. Results and discussion

AFM images (10 μm × 10 μm) of graphite electrode at OCV state and after cathodic polarization at 0.05 V versus Li/Li^+ in various electrolyte solutions are shown in Fig. 3. The surface of MCMB was observed as an assemblage of particles of 1.6–3.5 μm in size with many smaller particles about 0.5 μm in size at OCV. After cathodic polarization to 0.05 V at which lithium intercalated into graphene layers to form a graphite intercalation compound (GIC, C_6Li), a large expansion of MCMB particles was observed especially in the $LiPF_6$-solution (Fig. 3b). On the other hand, a small morphological change was observed in the $LiClO_4$-solution (Fig. 3f), and many obscure small ball-like particles about 600 nm in length and 500 nm in height were observed in the $LiBF_4$-solution (Fig. 3d). It was clearly shown that the anion of lithium salt strongly affects morphological changes of graphite at the first cathodic polarization. Consequently, not only solvents but also anions react to make something on graphite electrode surface.

Morphological changes in MCMB electrode in $LiPF_6$/EC + DMC at various potentials are shown in Fig. 4. AFM images (8 μm × 8 μm area) of almost the same position on the electrode was selected to observe morphological changes distinctly. It was observed that the morphology of MCMB particle changed from about 1.5 V versus Li/Li^+ at the first cathodic polarization. Although it was reported that the reduction of solvents mainly occurs at potentials lower than 1.0 V and the formation of first and second stages Li-GIC (C_6Li, $C_{12}Li$) occurs below 0.5 V [26], a small change in morphology was observed between 2.0 and 1.5 V. At 1.5 V (Fig. 4b), the particles expanded by about 350 nm in height from the OCV state (Fig. 4a). Then, the expansion of particles increased to about 670 nm at 1.0 V (Fig. 4c), and 915 nm at 0.05 V (Fig. 4e). This large expansion of particle remained about 870 nm even after anodic polarization to 1.0 V (Fig. 4f). These changes correspond to those of hard MCMB particles, not to a swelling of binder-resins or reduction products of solvents, because there are few scratching traces of resins or polymeric products in these AFM images. It is difficult to understand that these large and irreversible morphological changes occurred around 1.0 V, because the MCMB particle is not a single crystal and the electrode is a compound electrode. I think that the phenomenon which occurred over 1.0 V correspond to the formation and the decomposition of a ternary graphite intercalation compound. There are a few reports on a ternary lithium graphite intercalation compound (GIC) [27–29].

Besenhard et al. reported that solvated lithium ion is intercalated into graphene layers to form a ternary lithium GIC (C_nLi(sol)$_y$) in $LiClO_4$/EC + dimethoxy ethane (DME) and the decomposition of this ternary GIC (C_nLi(sol)$_y$) results in a drastic expansion of graphite matrix by about 150–200% as follows [27]:

$$C_n + \mathrm{Li(sol)}_y^+ + \mathrm{e}^- \rightarrow C_n\mathrm{Li(sol)}_y \quad (1)$$

$$C_n\mathrm{Li(sol)}_y \rightarrow C_n\mathrm{Li} + (y - z)(\mathrm{sol}) + z(\mathrm{pro}) \quad (2)$$

where, C_n: graphite matrix; (sol): solvent; Li(sol)$_y$, Li(sol)$_y^+$: solvated lithium or lithium ion; (pro): decomposition product.

The co-intercalation of solvent with lithium into graphite matrix was studied by Schoderböck and Boehm [29]. It was reported that co-intercalation of solvent into Madagascar flake graphite in $LiClO_4$/dimetyl sulfoxide (DMSO) system, and the intercalation/de-intercalation of lithium at low concentration level, such as $C_{72}Li$ or $C_{120}Li$, occurred in the range from 1.5 to 1.0 V versus Li/Li^+.

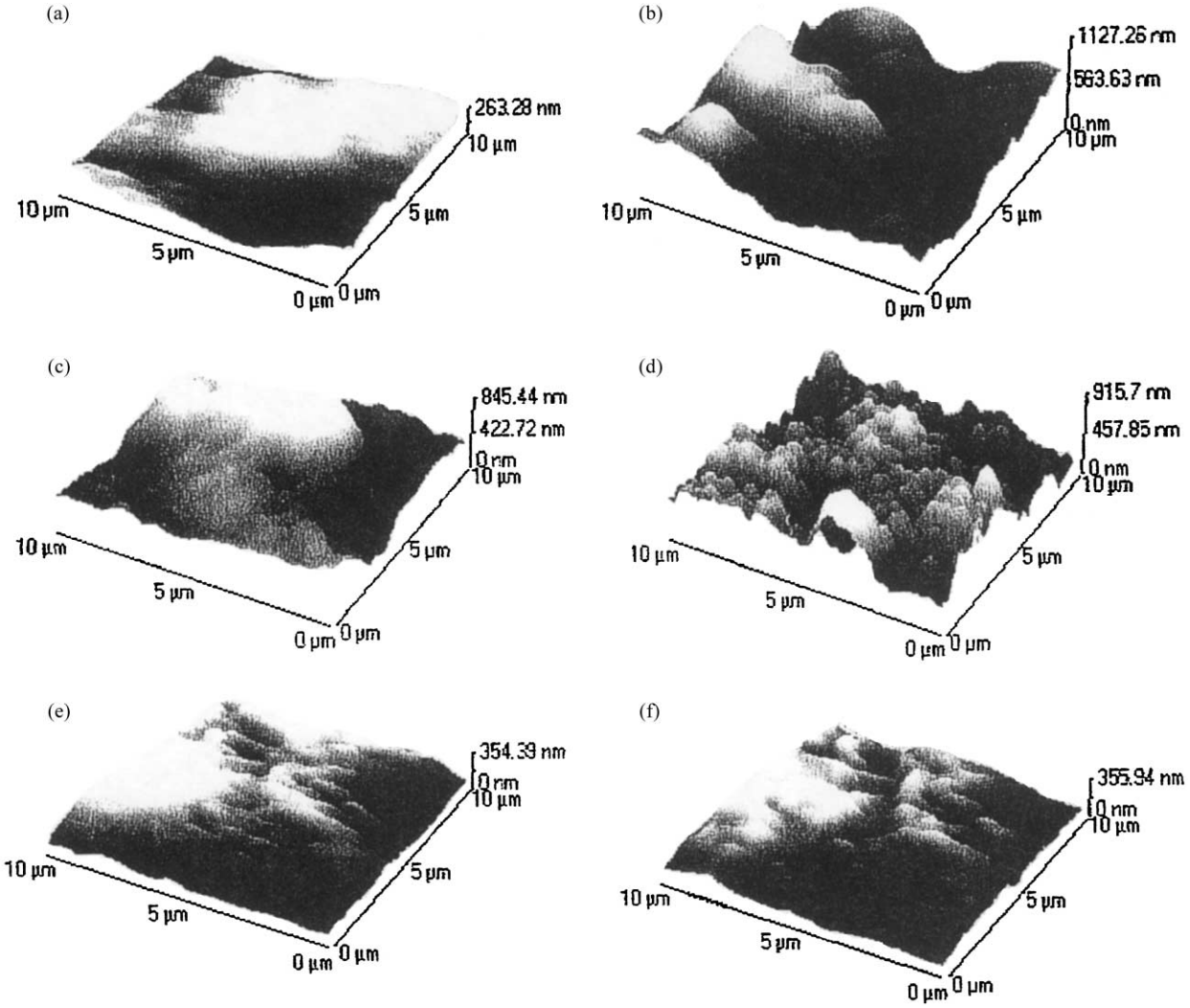

Fig. 3. A comparison between morphological changes of graphite electrodes from OCV to 0.05 V vs. Li/Li^+ in each electrolyte solution by in situ AFM observation. Area = 10 μm × 10 μm, (a) and (b) in $LiPF_6$/EC + DMC; (c) and (d) in $LiBF_4$/EC + DMC; (e) and (f) in $LiClO_4$/EC + DMC. (a, c, and e) At OCV; (b, d, and f) at 0.05 V vs. Li/Li^+.

Consequently, the expansion of MCMB particles at 1.5 (Fig. 4b) and 1.0 V (Fig. 4c) correspond to the formation of a ternary GIC. The decomposition of the ternary GIC correspond to the morphological changes between 1.0 and 0.5 V, because the formation of binary Li-GIC (C_6Li, $C_{12}Li$) occurs below 0.5 V. The result of in situ AFM observation (Fig. 4) is consistent with the phenomena reported by Besenhard et al. [27].

It was proved in previous AFM experiments [30] that polymeric materials, such as SBR binder-resin or larger organic compounds, make draggled or trailing lines in AFM measurements, and obtained AFM image becomes vague or obscure. However, there are few draggled lines in the AFM images obtained and the AFM images are very clear and distinct in this study. Therefore, it is concluded that the observed drastic expansion occurred in MCMB particle itself. In order to exhibit the influence of SBR binder-resin or polymeric reduction products, lateral force microscopy (LFM) measurements were carried out with AFM observation. AFM and LFM images of MCMB composite electrode at OCV and at 1.0 V versus Li/Li^+ in $LiPF_6$/EC + DMC are shown in Fig. 5. LFM images reflect the bending and twisting of the cantilever when the probe moves on the surface of sample. Therefore, LFM images indicate the difference in surface friction force corresponding to various surface species, that is, the degree of surface homogeneity and uniformity on a flat and smooth sample. LFM images can be obtained with AFM images for the same scanning area, but the cantilever is affected by the bending interaction due to topography. When the sample has a rough surface, LFM images are also influenced by topography of the sample. In the case of this composite electrode, MCMB particles and SBR binder-resin should have different friction forces, but the roughness of the sample is larger than 1 μm. Consequently, the LFM images in Fig. 5 not only indicate the distribution of graphite and binder-resin on electrode

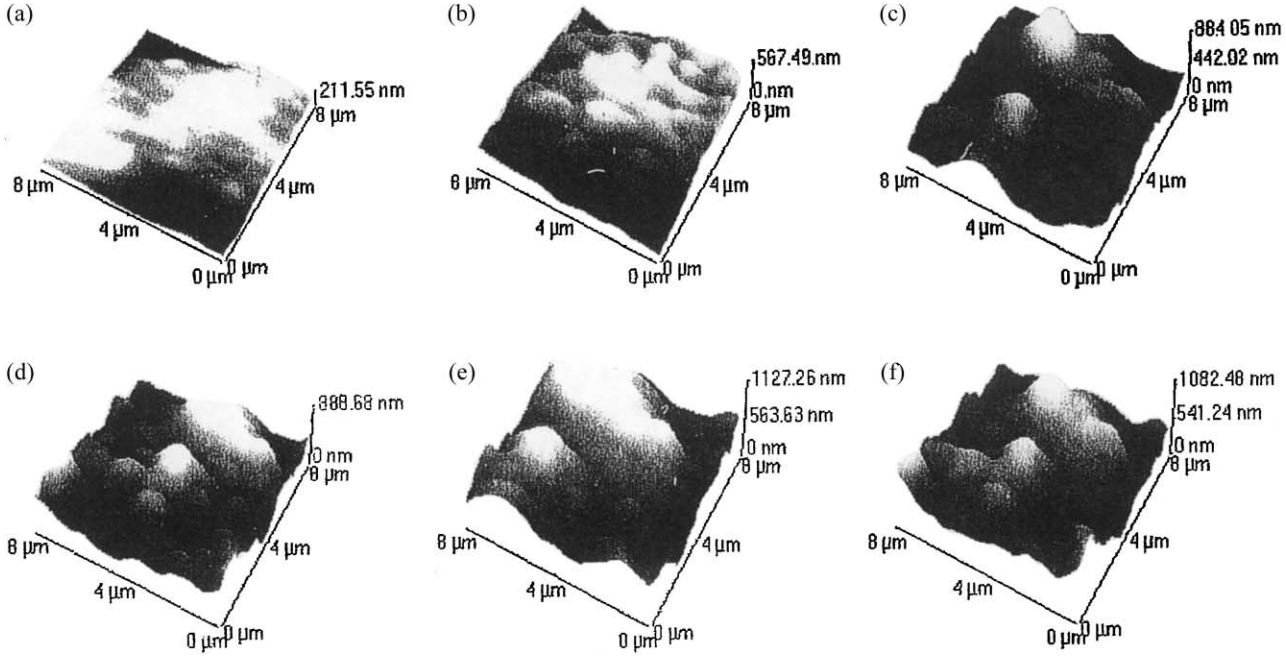

Fig. 4. Morphological changes of graphite electrode at various potentials in $LiPF_6$/EC + DMC. Area = 8 μm × 8 μm, (a) at OCV; (b) 1.5 V; (c) 1.0 V; (d) 0.5 V; (e) 0.05 V; (f) 1.0 V vs. Li/Li^+.

surface, but also are affected by the surface topography. The LFM image at OCV presents a somewhat lighter part at the left-hand side and the darker part at the center of the image (Fig. 5b), which may be corresponding to SBR binder-resin. The LFM image at 1.0 V presents a pattern like a contour line, which is caused by an interference of the laser beam. Thus, the expanded particle (the right-lower part in Fig. 5d) shows a very complicated image, but it is

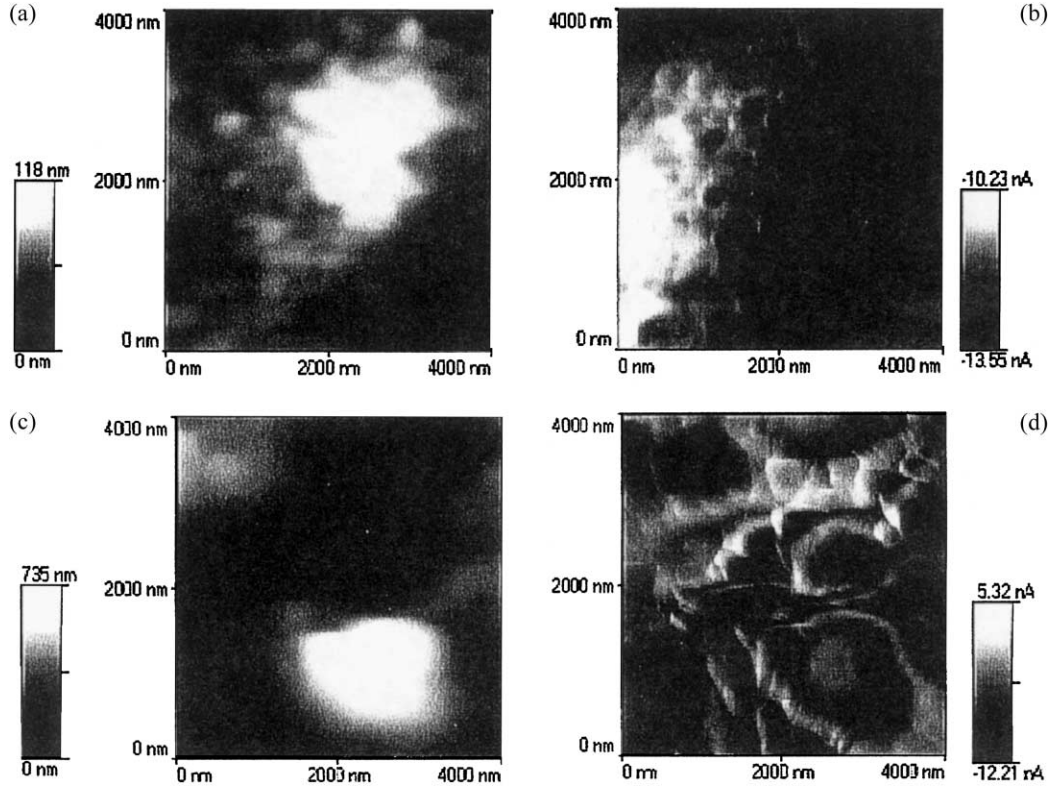

Fig. 5. AFM and (b, d) LFM images of graphite electrode in $LiPF_6$/EC + DMC. (a and b) OCV; (c and d) 1.0 V vs. Li/Li^+.

distinguished from a mass of resin or the reduction products of solvents. If the expanded parts consist swelled binder-resin or the polymeric decomposition products, the LFM image will show the bright and dark parts of image. However, the LFM (Fig. 5d) of the particle shows the other distribution of brightness corresponding to the interference. Furthermore, this result is supported by the results of in situ DMFTIR spectroscopy on MCMB electrode, as shown later.

Consequently, these results of surface morphological changes indicate some important facts as follows.

1. The first morphological changes occurs even at potentials above 1.0 V versus Li/Li^+ (in the range of 1.5–1.0 V) in the first cathodic polarization, at which solvated lithium ion may be intercalated into graphene layer to form a ternary GIC ($C_nLi(sol)_y$).
2. The decomposition of ($C_nLi(sol)_y$) may occur at potentials between 1.0 and 0.5 V.
3. An expansion of graphite particles at the first cathodic polarization remains even after discharged to 1.0 V (after anodic polarization), at which almost all of lithium ions de-intercalate from graphene layers.
4. After the first drastic expansion occurs, morphological change of graphite is relatively small during the following charging–discharging cycles.

Morphological changes of MCMB composite electrode in $LiBF_4$/EC + DMC are shown in Fig. 6. Surface image after polarization to 0.05 V was quite different from that in the $LiPF_6$-solution. The surface of MCMB particles looked like a gathering of small semi-spheres about 500 nm in diameter after the first cathodic polarization (Fig. 6c). The expansion remained even after anodic polarization to 1.0 V (Fig. 6d), and the difference in height was about 10 nm. The morphological changes in MCMB particles started from over 1.0 V and the first drastic expansion remained during the following charging–discharging cycles. Therefore, these morphological change of graphite in the $LiBF_4$-solution are also caused by the formation and the decomposition of ($C_nLi(sol)_y$).

Similar morphological changes in MCMB electrode in $LiClO_4$/EC + DMC are shown in Fig. 7. The surface morphology of MCMB changed slightly even at 0.05 V versus Li/Li^+ and some expanded lines were observed by the cathodic polarization. The edges of graphene layers were expanded by the intercalation of lithium ion. An expansion of MCMB occurred at 1.0 V as raised lines and particles. This result of AFM in the $LiClO_4$ solution is similar to those of STM studies [21,22]. These expanded parts correspond to the edge parts of graphene plane as Besenhard suggested that the formation of a ternary GIC ($C_nLi(sol)_y$) and following decomposition of ($C_nLi(sol)_y$) at the edge parts of graphene layers [27].

These results of AFM indicate that lithium salt (anion) considerably affects morphological changes of MCMB particle at the first cathodic polarization. The difference in morphological change is related to the interfacial reaction on MCMB particle in each solution. Therefore, it is very important to understand the interfacial reactions on MCMB electrode in each solution, and then they were investigated by in situ FTIR spectroscopy.

A comparison between DMFTIR spectra of mixed solvent (EC + DMC, Fig. 8a) and electrolyte solution ($LiPF_6$/EC + DMC, Fig. 8b) on MCMB electrode is presented in Fig. 8, together with the subtractive spectrum (Fig. 8c) between them. Similar subtractive spectra are also shown in the cases of $LiBF_4$-solution (Fig. 8d) and $LiClO_4$-solution

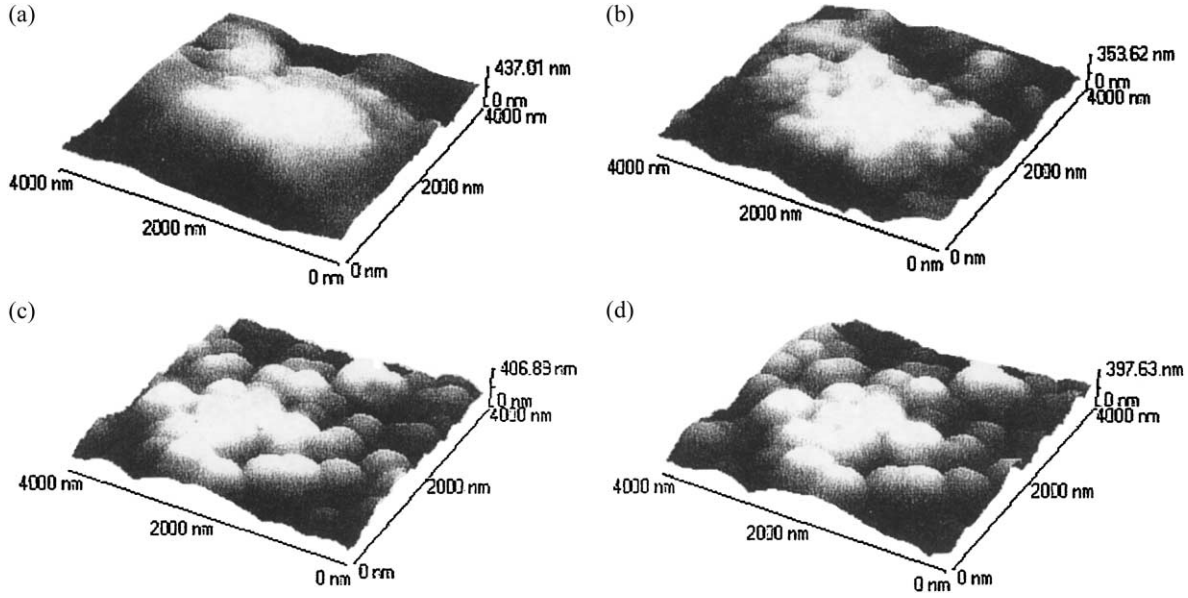

Fig. 6. AFM images of graphite electrode at various potentials in $LiBF_4$/EC + DMC. Area = 4000 nm × 4000 nm, (a) at OCV; (b) 1.0 V; (c) 0.05 V; (d) 1.0 V vs. Li/Li^+.

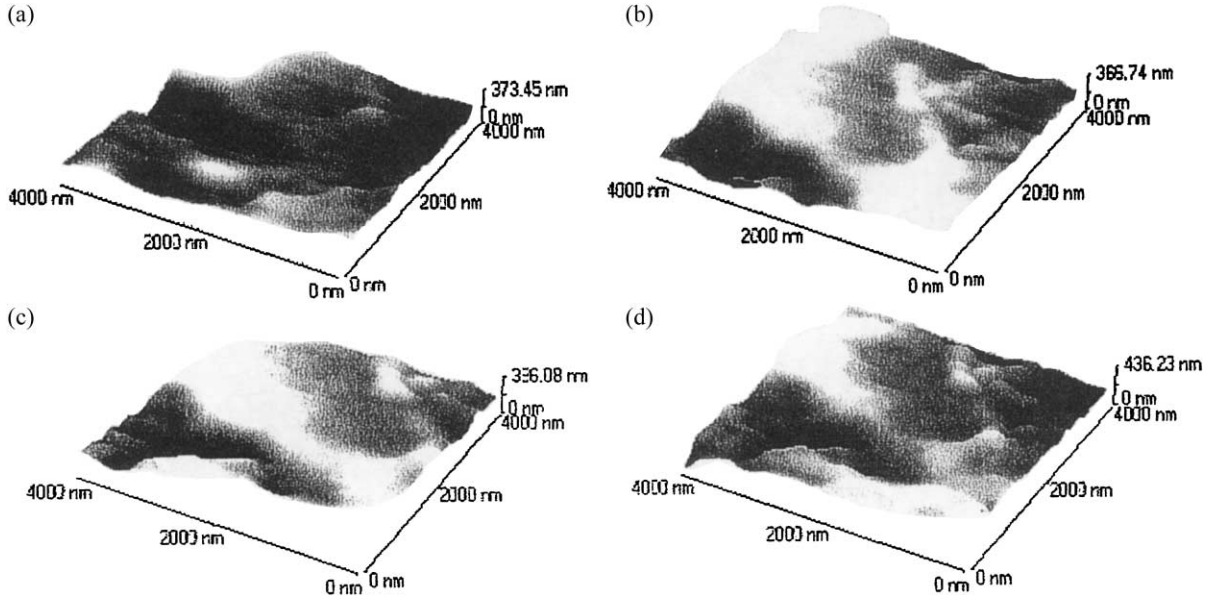

Fig. 7. AFM images of graphite electrode at various potentials in $LiClO_4$/EC + DMC. Area = 4000 nm × 4000 nm, (a) at OCV; (b) 1.0 V; (c) 0.05 V; (d) 1.0 V vs. Li/Li^+.

(Fig. 8e). A major peak in both DMFTIR spectra (Fig. 8a and b) is observed at 1748 cm^{-1}, which is assigned to the C=O asymmetric stretching vibration of carbonyl group

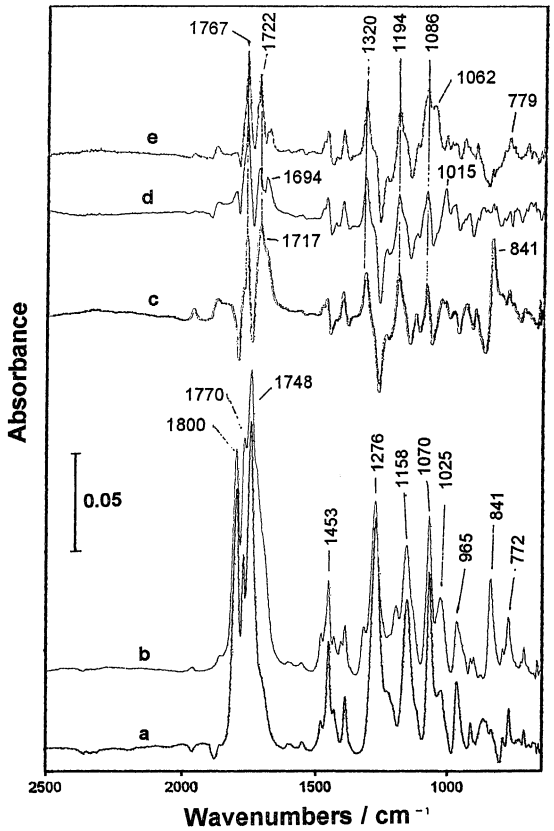

Fig. 8. Comparison between DMFTIR spectra of (a) solvent (EC + DMC) and (b) electrolyte solution ($LiPF_6$/EC + DMC), and (c–e) each subtractive spectrum between solvent and electrolyte solution on graphite electrode at OCV. (c) $LiPF_6$-solution; (d) $LiBF_4$-solution; (e) $LiClO_4$-solution.

($\nu_{C=O}$) of DMC [15]. Upward peaks are observed at 1800 and 1770 cm^{-1} and they are assigned to $\nu_{C=O}$ of EC [15]. Other peaks at 1276, 1158, and 1070 cm^{-1} are assigned to ν_{C-O-C} and ν_{C-O} of solvents (EC and DMC) [15]. It was reported that the decomposition of electrolyte occurs on carbon and lithium as follows [7–9].

$$LiPF_6 \rightarrow LiF + PF_5 \quad (3)$$

$$PF_5 + H_2O \rightarrow PF_3O + 2HF \quad (4)$$

$$PF_5 + 2xLi^+ + 2xe^- \rightarrow Li_xPF_{5-x} + xLiF \quad (5)$$

$$PF_3O + 2xLi^+ + 2xe^- \rightarrow Li_xPF_{3-x}O + xLiF \quad (6)$$

$$LiPF_6 + 2H_2O \rightarrow LiF + H[PF_2O_2] + 3HF \quad (7)$$

$$LiBF_4 + xLi^+ + xe^- \rightarrow Li_{1-x}BF_{4-x} + xLiF \quad (8)$$

$$LiClO_4 + 2Li^+ + 2e^- \rightarrow LiClO_3 + Li_2O \quad (9)$$

It was reported that the spectrum of $LiPF_6$-solution has characteristic peaks at 1050 cm^{-1} (ν_{P-O}) and 850–830 cm^{-1} (ν_{P-F}), that of $LiBF_4$-solution at 1030–1020 cm^{-1} (ν_{B-F}), and that of $LiClO_4$-solution around 1050 cm^{-1} (ν_{Cl-O}), and each peak is related to the decomposition product of each salt [7–9]. Accordingly, the characteristic peak at 841 cm^{-1} in spectrum 8c (Fig. 8c) is ascribed to ν_{P-F}, the peak at 1015 cm^{-1} in spectrum 8d (Fig. 8d) to ν_{B-F}, and the peak at 1062 cm^{-1} in spectrum 8e (Fig. 8e) to ν_{Cl-O}. The assignment of each peak of solvent (EC and DMC) in DMFTIR and IRAS spectra is shown in Table 1 together with that of other solvents, diethyl carbonate (DEC) and dimethoxy ethane (DME). New upward peaks are observed at 1767, 1722, 1320, 1086, and 1194 cm^{-1} in each subtractive spectrum and they correspond to the change in solvents by dissolution of lithium salt, such as the solvation of lithium ion.

Table 1
Assignment of each peak in DMFTIR and IRAS spectra of solvents[a]

	EC		DMC		DEC		DME	
	DM	(IRAS)	DM	(IRAS)	DM	(IRAS)	DM	(IRAS)
$\nu_{C=O}$	1800	(1792)	1752	(1728)	1741	(1724)	–	(–)
	1772	(1765)						
δ_{CH,CH_3}	1480	(1480)	1452	(1446)	1441	(1438)	1452	(1452)
	1388	(1386)	1432	(1430)	1373	(1370)	1365	(1365)
$\nu_{C–O–C}$	1230		1270		1251		1245	
$\nu_{C–O}$	1158	(1127)	1135	(1178)	1142	(1183)	1190	(1190)
	1070	(1040)	1093	(1137)	1090	(1086)	1107	(1110)
							1058	(1083)
$\nu_{C–C}$	1029		–	(–)	1017		1023	(1024)
	990	(950)	968			(960)	980	(980)
	970	(910)				(897)	935	(935)
δ_{CO_3}	826	(830)	870	(897)	853	(841)	–	(–)
						(820)		

[a] DEC: diethyl carbonate; DME: dimethoxy ethane.

IRAS spectrum of mixed solvent (EC + DMC) is shown in Fig. 9, together with the subtractive spectrum 9b (Fig. 9b) between solvent and electrolyte solution ($LiPF_6$/EC + DMC). Similar subtractive spectra in the $LiBF_4$-solution and in the $LiClO_4$-solution are also shown in Fig. 9c and d, respectively. The subtractive spectrum of 9b (Fig. 9b) ($LiPF_6$-solution) presents large downward peaks at around 882 and 860 cm^{-1} together with other downward peaks at 1790, 1724, 1235, 1116, 1002, and 924 cm^{-1}. On the other hand, upward peaks are observed at 1688, 1320, 1190, 1086, and 810 cm^{-1} in spectrum 9b (Fig. 9b). The other subtractive spectra (Fig. 9c and d) also give similar upward peaks at 1688 cm^{-1} ($\nu_{C=O}$), 1320 cm^{-1} ($\nu_{C=O}$), 1190 cm^{-1} ($\nu_{C–O}$), 1086 cm^{-1} ($\nu_{C–O}$), and downward peaks at 1235 cm^{-1} ($\nu_{C–O–C}$) and 1116 cm^{-1} ($\nu_{C–O}$). Therefore, these peaks are related with the solvation of lithium ion. Furthermore, the peaks at 1320 and 1086 cm^{-1} are consistent with those of DMFTIR spectra (Fig. 8c–e), and the peak at 1190 cm^{-1} is shifted from 1194 cm^{-1} in DMFTIR spectra. The downward peaks at around 882, 860, 1002, and 924 cm^{-1} in spectrum 9b (Fig. 9b) are characteristic peaks in the $LiPF_6$-solution. They are not assigned, but they correspond to the changes of solvents by addition (dissolution) of $LiPF_6$.

Then, IRAS spectra of some $LiPF_6$-solutions (the concentration of $LiPF_6$ was changed from 0.01 to 1 mol dm^{-3}) were measured, and each subtractive spectrum between solution and mixed solvent is shown in Fig. 10. Subtractive IRAS spectrum of 10d (Fig. 10d) (0.01 mol dm^{-3} $LiPF_6$/EC + DMC) shows upward peaks at 1300, 994, and 816 cm^{-1}. As the concentration of $LiPF_6$ increased, the absorbance of the peak around 816–810 cm^{-1} increased, and it is ascribed to $\nu_{P–F}$ of $LiPF_6$. The absorbances of peaks at 1688 cm^{-1} ($\nu_{C=O}$), 1320 cm^{-1} ($\nu_{C=O}$), 1190 cm^{-1} ($\nu_{C–O}$), 1086 cm^{-1} ($\nu_{C–O}$), and 720 cm^{-1} increased with the concentration of Li-salt, and those of peaks at 1790 cm^{-1} ($\nu_{C=O}$), 1235 cm^{-1} ($\nu_{C–O–C}$) and 1116 cm^{-1} ($\nu_{C–O}$) decreased. These results are consistent with those of Fig. 9,

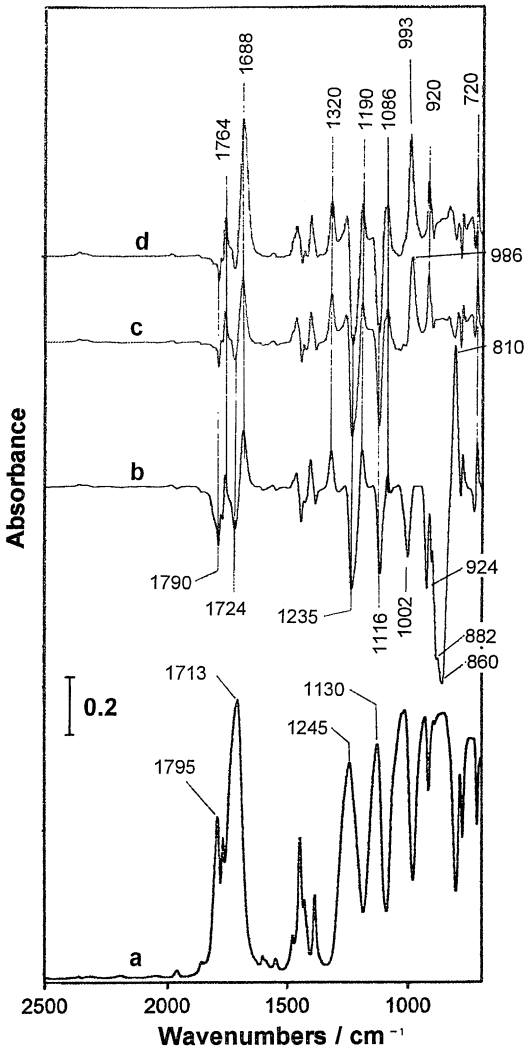

Fig. 9. IRAS spectrum of (a) solvent (EC + DMC) and each subtractive IRAS spectra between solvent and electrolyte solution on graphite electrode at OCV. (b) $LiPF_6$-solution; (c) $LiBF_4$-solution; (d) $LiClO_4$-solution.

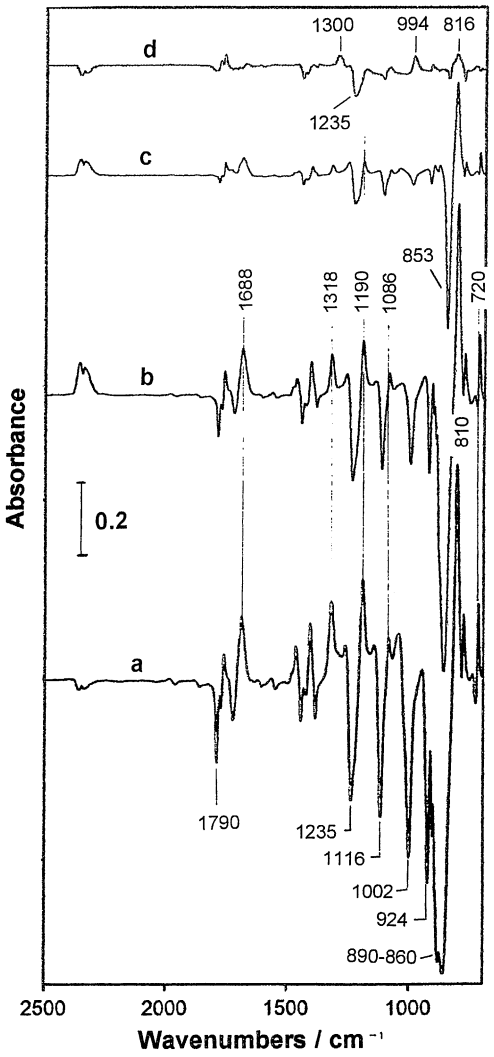

Fig. 10. Subtractive IRAS spectra between solvent (EC + DMC) and each $LiPF_6$-solution on graphite electrode at OCV. Concentration of $LiPF_6$: (a) 1 mol dm^{-3}; (b) 0.5 mol dm^{-3}; (c) 0.1 mol dm^{-3}; (d) 0.01 mol dm^{-3}.

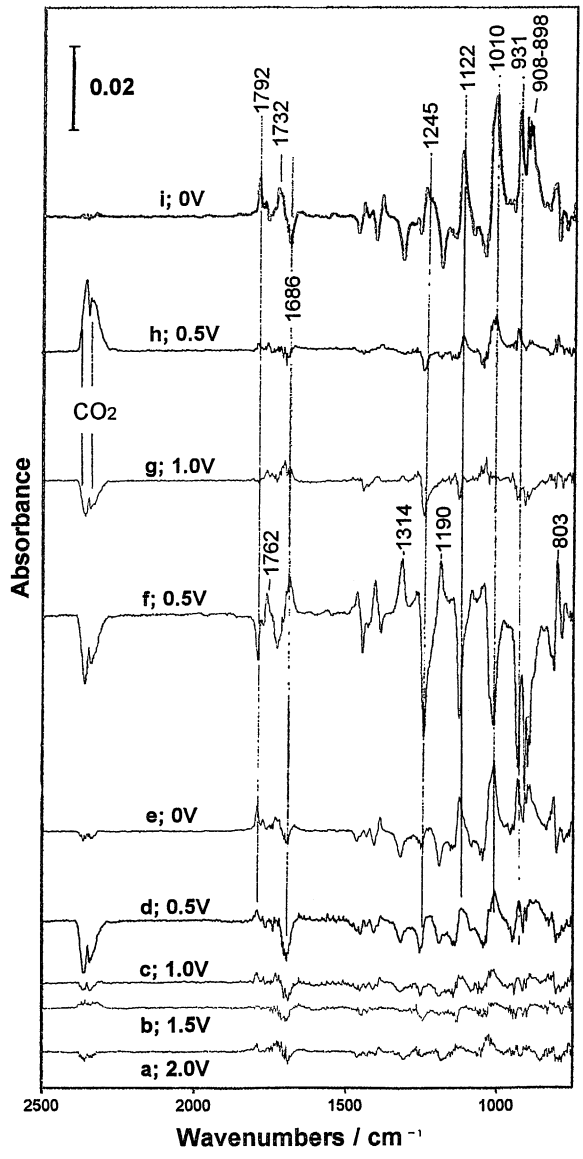

Fig. 11. Changes in IRAS spectra of 1 mol dm^{-3} $LiPF_6$/EC + DMC at various potentials: (a) 2.0 V; (b) 1.5 V; (c) 1.0 V; (d) 0.5 V; (e) 0 V; (f) 0.5 V; (g) 1.0 V; (h) 0.5 V; (i) 0 V vs. Li/Li^+.

and these upward peaks are related with the solvation of lithium ion. On the other hand, characteristic peaks of $LiPF_6$-solution are observed from 1002 to 860 cm^{-1} as downward peaks. Spectrum 10c (Fig. 10c) (0.1 mol dm^{-3}) shows a downward peak at 853 cm^{-1}, and the absorbance of this peak decreased as the concentration of $LiPF_6$ increased. The peak of 853 cm^{-1} became downward broad peak from 890 to 860 cm^{-1} in the spectrum of 1 mol dm^{-3} $LiPF_6$-solution (Fig. 10a). This phenomenon is observed only in the $LiPF_6$-solution, that is, higher concentration of $LiPF_6$ makes a large change in the configuration of solvents. Therefore, PF_6-anion makes strong interactions with solvents, which gives downward peaks at around 890, 860, 1002, and 924 cm^{-1}.

IRAS spectra of 1 mol dm^{-3} $LiPF_6$/EC + DMC on MCMB electrode at various potentials are shown in Fig. 11. Each spectrum was obtained using the interferogram of the previous one as a reference, as described in the previous studies [17,18]. Small changes in the spectrum during polarization are observed at 2.0 V versus Li/Li^+ (Fig. 11a), and obvious changes are observed at 0.5 V (Fig. 11d). Each IRAS spectrum during the first cathodic polarization (Fig. 11a–e) looks like a similar spectrum which has the same upward peaks and downward peaks. As shown in Figs. 9 and 10, the solvation of lithium ion in EC + DMC gives upward peaks at 1688, 1320, and 1190 cm^{-1}, and downward peaks at 1235 and 1116 cm^{-1}, and the interaction between PF_6-anion and solvents makes downward peaks at 1002, 924, 882, and 860 cm^{-1}. Upward peaks at 1792, 1732, 1245, 1122, 1010, 931, and around 900 cm^{-1} in spectrum 11e (Fig. 11e) (0 V) have changed from downward peaks in spectrum 9b (Fig. 9b). Upward peaks in spectrum 11f (Fig. 11f) (0.5 V) have showed similar upward peaks in

spectrum 9b (Fig. 9b). Accordingly, IRAS spectra indicates mainly changes in the concentration of $LiPF_6$ in the phase which is near the electrode about some micrometre. Because p-polarized IR beam passes through the solution layer between IR window and electrode (thickness $< 10\ \mu m$) twice, the strong absorption of solvent in the bulk phase conceals the interfacial phenomena. Spectrum 11i (Fig. 11i) which was obtained at 0 V in the second polarization shows a similar pattern to spectrum 11e (Fig. 11e).

A previous FTIR study [15] reported that the reduction product of EC is $(CH_2OCO_2Li)_2$ which has the peaks at 1650 cm^{-1} ($\nu_{C=O}$), 1450 to 1400 cm^{-1} (δ_{CH_2}), 1350 to 1290 cm^{-1} ($\nu_{C=O}$), 1100 to 1070 cm^{-1} (ν_{C-O}), and 840 to 820 cm^{-1} (δ_{OCO_2}). It was also reported that the decomposed product of DMC is CH_3OCO_2Li which has the peaks at 1647 cm^{-1} ($\nu_{C=O}$), 1490 cm^{-1} (δ_{CH_3}), 1353 cm^{-1} ($\nu_{C=O}$), 1105 cm^{-1} (ν_{C-O}), 984 cm^{-1} (ν_{C-C}), and 863 cm^{-1} (δ_{OCO_2}) [15]. It has also reported that a dominant product on the electrode is $(CH_2OCO_2Li)_2$ in EC + DMC solutions. If $(CH_2OCO_2Li)_2$ is the dominant product in the interfacial reaction, the peak at 1650 cm^{-1}, which is assigned to $\nu_{C=O}$ of $(CH_2OCO_2Li)_2$, will be the major upward peak in the spectrum. Although the upward peaks due to $\nu_{C=O}$ are observed at 1792 and 1732 cm^{-1} in spectra 11e and i (Fig. 11e and i), they correspond to solvent (EC) and the change by the solvation of lithium ion. The peaks of CO_2 increased in spectrum 11h (Fig. 11h) and it suggests that the decomposition of solvents or products has occurred even after the first cathodic polarization.

IRAS spectra of $LiBF_4$-solution obtained in a similar manner are presented in Fig. 12. It was found that the peaks at 1245 and 1448 cm^{-1} are downward, and the peaks at 1677, around 996 and 811 cm^{-1} are upward, continuously. Major upward peak in spectrum 12i (Fig. 12i) (0 V) is observed at 1677 cm^{-1}, which is ascribed to $\nu_{C=O}$ of $ROCO_2Li$, and the other peaks at 1126, 996, 851 cm^{-1} are ascribed to ν_{C-O}, ν_{C-C}, and δ_{OCO_2} of $ROCO_2Li$, respectively [15]. Downward peaks at 1245 and 1448 cm^{-1} are ascribed to ν_{C-O-C} and δ_{CH} of EC, because they are often observed in spectra of the solution containing EC. These downward peaks indicate that the decomposition of EC occurred during polarization. The dominant reduction product on MCMB electrode in the $LiBF_4$-solution was $ROCO_2Li$, which has the peaks at 1677 cm^{-1} ($\nu_{C=O}$), 1126 cm^{-1} (ν_{C-O}), 996 cm^{-1} (ν_{C-C}) and 851 cm^{-1} (δ_{OCO_2}). It is generally accepted that solvents decompose to form the surface passive layers on graphite electrode during the first charging process in a lithium-ion battery. Consequently, further decomposition of solvents is protected by these passive layers. IRAS spectrum 12i (Fig. 12i) obtained in the second cathodic polarization showed that the peaks of reduction product, such as 1677 cm^{-1} ($\nu_{C=O}$), 996 cm^{-1} (ν_{C-C}) and 851 cm^{-1} (δ_{OCO_2}), increased much more than those of in spectrum 12e (Fig. 12e). Therefore, this result indicates that the surface passivation on MCMB electrode is insufficient and the reduction of solvent has repeated at the second cycle in $LiBF_4$/EC + DMC.

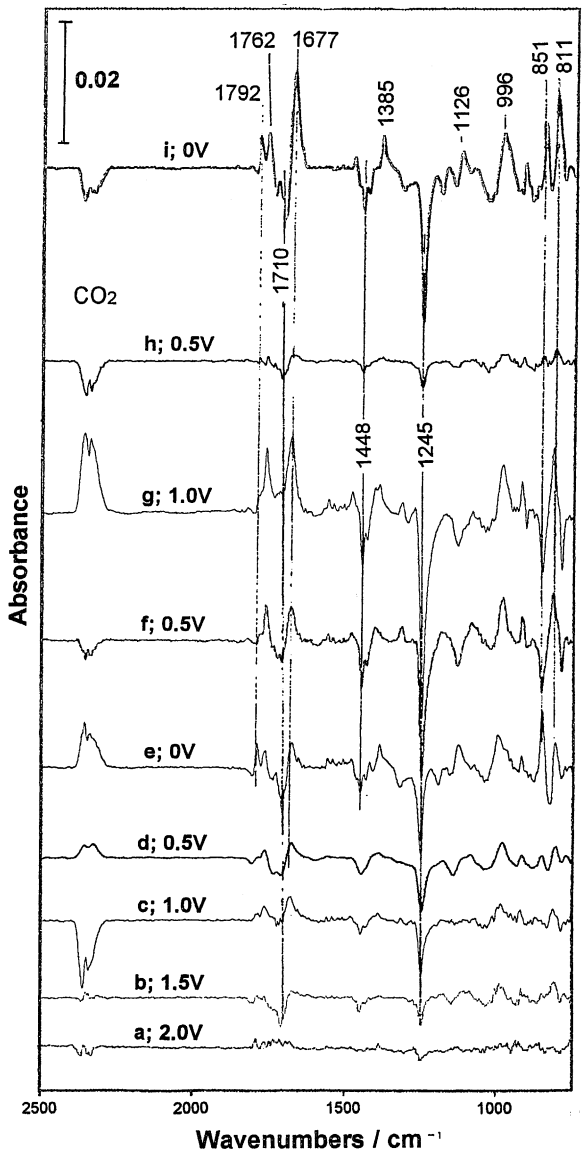

Fig. 12. Changes in IRAS spectra of 1 mol dm^{-3} $LiBF_4$/EC + DMC at various potentials: (a) 2.0 V; (b) 1.5 V; (c) 1.0 V; (d) 0.5 V; (e) 0 V; (f) 0.5 V; (g) 1.0 V; (h) 0.5 V; (i) 0 V vs. Li/Li^+.

IRAS spectra of $LiClO_4$-solution obtained in a similar manner are presented in Fig. 13. IRAS spectra 13e and f (Fig. 13e and f) showed interesting behavior, that is, downward peaks at 0 V (1682, 1317, and 991 cm^{-1}) became upward at 0.5 V. On the other hand, upward peaks at 0 V (around 1230, and 1130 cm^{-1}) became downward at 0.5 V. Therefore, spectrum 13f (Fig. 13f) looks like the reverse form of spectrum 13e (Fig. 13e). Major upward peaks at 1682, 1317, and 991 cm^{-1} in Fig. 13f (0.5 V) have shifted from 1688, 1320, and 993 cm^{-1} in spectrum 9d (Fig. 9d), which correspond to the solvation of lithium ion. On the other hand, major upward peaks at 1130 and around 1230 cm^{-1} are observed in spectra at 0 V (Fig. 13e and i), and they have also shifted from 1116 and 1235 cm^{-1} in spectrum 9d (Fig. 9d). The peak at 1682 cm^{-1} in Fig. 13f

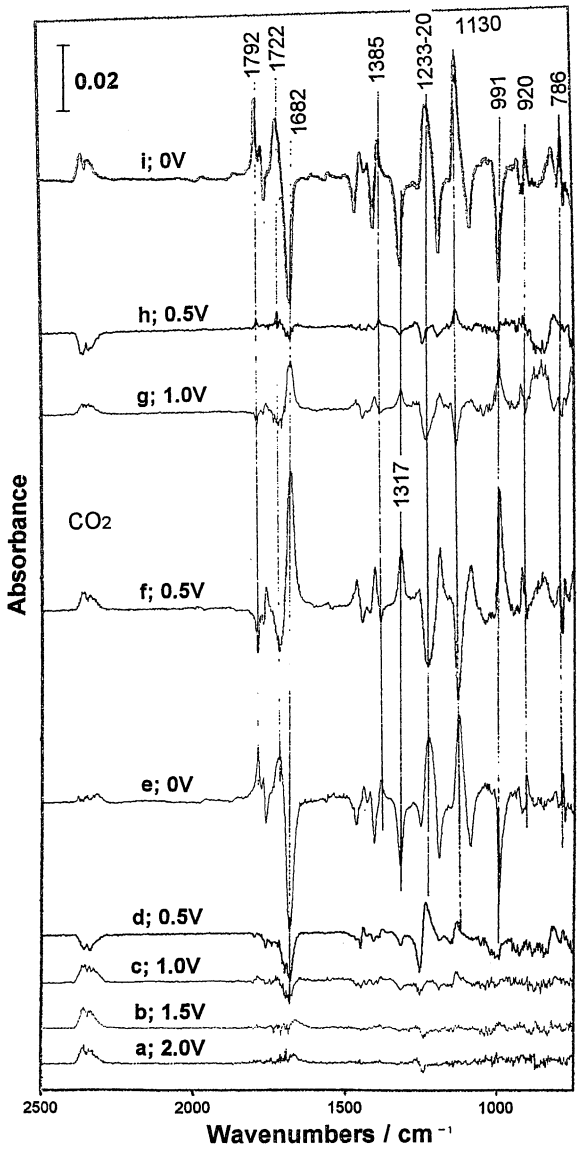

Fig. 13. Changes in IRAS spectra of 1 mol dm^{-3} $LiClO_4$/EC + DMC at various potentials: (a) 2.0 V; (b) 1.5 V; (c) 1.0 V; (d) 0.5 V; (e) 0 V; (f) 0.5 V; (g) 1.0 V; (h) 0.5 V; (i) 0 V vs. Li/Li^+.

(0.5 V) may be ascribed to $\nu_{C=O}$ of $ROCO_2Li$ of the reduction product, but it decreased at 0 V (Fig. 13e and i). Therefore, upward peaks in spectrum 13f (Fig. 13f) (0.5 V) correspond to the increase in concentration of lithium ion near the electrode (by de-intercalation). Upward peaks in spectrum 13e (Fig. 13e) (0 V) also correspond to an increase in concentration of free solvent molecules near the electrode (by intercalation). IRAS spectra in the $LiClO_4$-solution indicate the change in the concentration of lithium ion near the electrode.

DMFTIR spectrum of 1 mol dm^{-3} $LiPF_6$/EC + DMC obtained at 0V versus Li/Li^+ is shown in Fig. 14a, together with subtractive spectra (Fig. 14b–d) between at OCV and at 0 V ((b) $LiPF_6$-solution; (c) $LiBF_4$-solution; (d) $LiClO_4$-solution). DMFTIR spectra at 0 V were measured after three cycles (from 1 to 0 V, by potentionstatic polarization), and

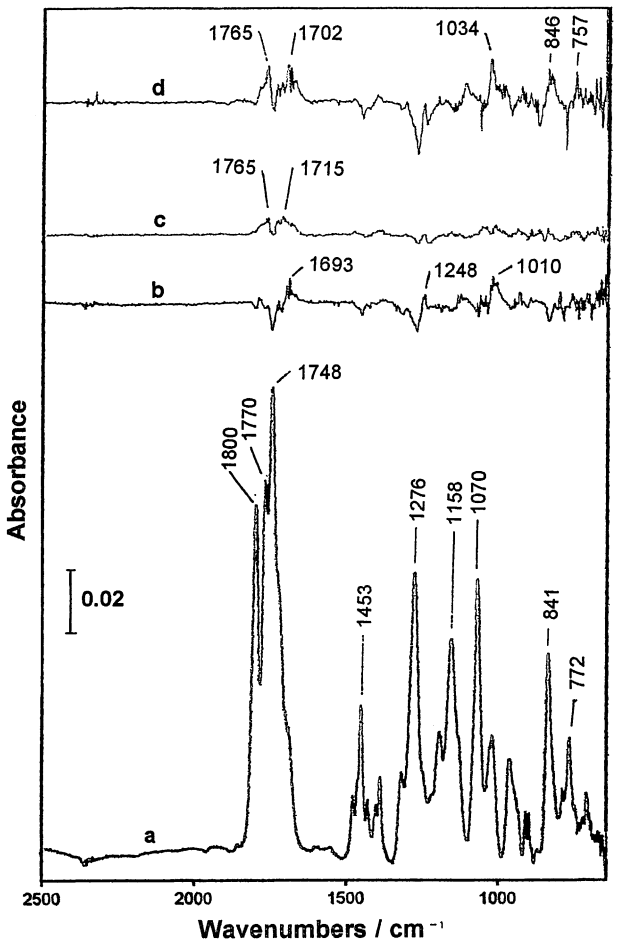

Fig. 14. DMFTIR spectrum of (a) $LiPF_6$/EC + DMC at 0 V and (b–d) each subtractive spectrum between at OCV and at 0 V vs. Li/Li^+ on graphite electrodes. (b) $LiPF_6$-solution; (c) $LiBF_4$-solution; (d) $LiClO_4$-solution.

they look like similar spectra obtained at OCV (Fig. 8). Although the result of IRAS spectra indicated many peaks during the polarization as shown in Figs. 11–13, each subtractive DMFTIR spectrum shows very small changes. In the $LiClO_4$-solution, the subtractive spectrum 14d (Fig. 14d) presents upward new peaks at 1765, 1702, 1034, 846, and 757 cm^{-1}. Although these peaks are not consistent with the result of IRAS spectra (Fig. 13), they may be ascribed to the peaks of $ROCO_2Li$, which are 1765 and 1702 cm^{-1} ($\nu_{C=O}$), 1034 cm^{-1} (ν_{C-O}), and 846 cm^{-1} (δ_{OCO_2}), respectively. This decomposition product ($ROCO_2Li$) exists on the surface of MCMB electrode, and forms the surface layer. In the $LiBF_4$-solution, the peaks at 1765 and 1715 cm^{-1} in DMFTIR spectrum 14c (Fig. 14c), which correspond to the reduction products on the electrode surface, may shift from the peaks at 1762 and 1710 cm^{-1} in IRAS spectrum 12g (Fig. 12g) (1.0 V). It indicates that the reduction products are dissoluble in the $LiBF_4$-solution and the surface passivation on MCMB electrode is insufficient. The peak at 1693 cm^{-1} in spectrum 14b (Fig. 14b) and peaks at 1765, 1715 cm^{-1} in spectrum 14c (Fig. 14c) are ascribed to $\nu_{C=O}$ of $ROCO_2Li$ of decomposition products on the

surface. Therefore, subtractive DMFTIR spectra indicate that the precipitated products on MCMB electrode may be lithium alkylcarbonates, but the amount of precipitate is small (from the comparison between the absorbances of solvents and those of products). DMFTIR spectra also suggest that morphological changes observed by in situ AFM mainly correspond to the expansion of MCMB particles and not to the reduction products.

4. Conclusion

A drastic expansion of graphite particles was found especially in the $LiPF_6$-solution at the first cathodic polarization by in situ AFM. A large expansion of graphite particles and the potential range ($1.5 \sim 1.0$ V), in which the expansion started, suggest that co-intercalation of solvated lithium ion occurs to form a ternary GIC ($Li(sol)_yC_n$), followed by decomposition of this ternary GIC. This morphological change of graphite matrix is strongly affected by the anion of lithium salt. It may be related to the irreversible capacity loss at the first cycle. Consequently, smooth and continuous intercalation of lithium into graphene layers needs the broad entrance to perform de-solvation of lithium ion and proceed the intercalation into graphene layers. The results in this study suggest that the pretreatment of graphite to expand the edge part of graphene layers makes it possible to achieve some improvements, such as a higher specific capacity, a lower irreversible capacity loss, or a longer cycle life.

Results of DMFTIR spectroscopy indicate that the organic surface layer on graphite consists of precipitates of lithium alkylcarbonate as the reduction product of solvents, however, the amount of precipitates is not so much in each electrolyte solution. IRAS spectra of electrolyte solutions show that continuous decomposition of solvents occurs on graphite electrode especially in the $LiBF_4$-solution. As a result, it is concluded that the organic surface layer on graphite consists of a precipitate of lithium alkylcarbonates, however, it does not act enough as a passive layer to protect further reduction. Therefore, further reduction of solvents will be a little but continuously occurs on graphite electrodes, and it will cause a gradual reduction of capacity with charge/discharge cycles.

Acknowledgements

The author is indebted to the New Energy and Industrial Technology Development Organization for their support to this study.

References

[1] R. Fong, U. Von Sacken, J.R. Dahn, J. Electrochem. Soc. 137 (1990) 2009–2013.
[2] E. Peled, C. Menachem, D. Bar-Tow, A. Melman, J. Electrochem. Soc. 143 (1996) L4–7.
[3] Y. Matsumura, S. Wang, J. Mondori, J. Electrochem. Soc. 142 (1995) 2914–2918.
[4] A.N. Dey, B.P. Sullivan, J. Electrochem. Soc. 117 (1970) 222–224.
[5] Z.X. Shu, R.S. McMillan, J.J. Murray, J. Electrochem. Soc. 140 (1993) 922–927.
[6] M. Arakawa, J. Yamaki, J. Power Sources 54 (1995) 250–254.
[7] D. Aurbach, A. Zaban, J. Electrochem. Soc. 141 (1994) 1808–1819.
[8] D. Aurbach, A. Zaban, O. Chusid, I. Weissman, Electrochim. Acta 39 (1994) 51–71.
[9] D. Aurbach, A. Zaban, Y. Gofer, Y. Ein-Eli, I. Weissman, O. Chusid, O. Abramson, J. Power Sources 54 (1995) 76–84.
[10] K. Kanamura, H. Tamura, S. Shiraishi, Z. Takehara, J. Electroanal. Chem. 394 (1995) 49–62.
[11] K. Kanamura, H. Takezawa, S. Shiraishi, Z. Takehara, J. Electrochem. Soc. 144 (1997) 1900–1906.
[12] D. Aurbach, Y. Ein-Eli, O. Chusid, Y. Carmeli, M. Babai, H. Yamin, J. Electrochem. Soc. 141 (1994) 603–611.
[13] Y. Ein-Eli, B. Markovsky, D. Aurbach, Y. Carmeli, H. Yamin, S. Luski, Electrochim. Acta 39 (1994) 2559–2569.
[14] D. Aurbach, A. Zaban, A. Shechter, Y. Ein-Eli, E. Zinigrad, B. Markovsky, J. Electrochem. Soc. 142 (1995) 2882–2890.
[15] D. Aurbach, B. Markovsky, A. Shechter, Y. Ein-Eli, H. Cohen, J. Electrochem. Soc. 143 (1996) 3809–3820.
[16] G. Binnig, C.F. Quate, Ch. Gerber, Phys. Rev. Lett. 56 (1986) 930–933.
[17] K. Morigaki, N. Kabuto, K. Yoshino, A. Ohta, Power Sources 15, in: A. Attewell, T. Keily (Eds.), Proceedings of the International Power Sources Symposium Committee, 1995, pp. 267–283.
[18] K. Morigaki, A. Ohta, J. Power Sources 76 (1998) 159–166.
[19] K.A. Hirasawa, T. Sato, H. Asahina, S. Mori, J. Electrochem. Soc. 144 (1997) L81–84.
[20] A.C. Chu, J.Y. Josefowicz, G.C. Farrington, J. Electrochem. Soc. 144 (1997) 4161–4169.
[21] M. Inaba, Z. Siroma, A. Funabiki, Z. Ogumi, T. Abe, Y. Mizutani, M. Asano, Langmuir 12 (1996) 1535–1540.
[22] Z. Ogumi, Z. Siroma, Y. Kawatate, A. Funabiki, T. Abe, M. Inaba, in: Proceedings of the 2nd Korea–Japan Joint Seminar on Advanced Batteries, Extended Abstract, 1997, pp. 163–170.
[23] M. Tatsumi, FTIR no Kiso to Jissai, 2nd Edition, Tokyo kagaku doujin, Tokyo, 1994, pp. 112–128.
[24] W.N. Richmond, P.W. Faguy, R.S. Jackson, S.C. Weibel, Anal. Chem. 68 (1996) 621–628.
[25] K. Morigaki, T. Fujii, A. Ohta, Denki kagaku (presently Electrochemitry) 66 (1998) 824–830.
[26] T. Ohzuku, Y. Iwakoshi, K. Sawai, J. Electrochem. Soc. 140 (1993) 2490–2498.
[27] J.O. Besenhard, M. Winter, J. Yang, W. Biberacher, J. Power Sources 54 (1995) 228–231.
[28] M. Winter, P. Novak, A. Monnier, J. Electrochem. Soc. 145 (1998) 428–436.
[29] K. Schoderböck, H.P. Boehm, Synth. Met. 44 (1991) 239–246.
[30] K. Morigaki, T. Fujii, A. Ohta, Denki kagaku (presently Electrochemitry) 66 (1998) 1114–1122.